Molecular Crystals and Liquid Crystals

ISSN: 1542-1406 (Print) 1563-5287 (Online) Journal homepage: http://www.tandfonline.com/loi/gmcl20

Indolyl-substituted carbazole derivatives: Electrochemical and photophysical properties and computational studies

R. Keruckiene, D. Peckus, T. Tamulevicius, S. Tamulevicius, M. Daniels, W. Dehaen, J. Simokaitiene & J. V. Grazulevicius

To cite this article: R. Keruckiene, D. Peckus, T. Tamulevicius, S. Tamulevicius, M. Daniels, W. Dehaen, J. Simokaitiene & J. V. Grazulevicius (2016) Indolyl-substituted carbazole derivatives: Electrochemical and photophysical properties and computational studies, Molecular Crystals and Liquid Crystals, 640:1, 59-70, DOI: 10.1080/15421406.2016.1255517

To link to this article: http://dx.doi.org/10.1080/15421406.2016.1255517

MOLECULAR CRYSTALS AND LIQUID CRYSTALS
2016, VOL. 640, 59–70
http://dx.doi.org/10.1080/15421406.2016.1255517

Taylor & Francis
Taylor & Francis Group

Indolyl-substituted carbazole derivatives: Electrochemical and photophysical properties and computational studies

R. Keruckiene[a], D. Peckus[b], T. Tamulevicius[b], S. Tamulevicius[b], M. Daniels[c], W. Dehaen[c], J. Simokaitiene[a], and J. V. Grazulevicius[a]

[a]Kaunas University of Technology, Department of Polymer Chemistry and Technology, Kaunas, Lithuania; [b]Kaunas University of Technology, Institute of Material Science, Kaunas, Lithuania; [c]Katholieke University Leuven, Department of Chemistry, Leuven, Belgium

ABSTRACT

A series of new indolyl-substituted carbazole derivatives were synthesized and their properties were studied. All the final compounds form molecular glasses. They absorb electromagnetic radiation in the range of 200–400 nm and emit in the range of 420–600 nm. The electrochemical properties of the derivatives were found to be determined by the nitro group attached to indole moiety. Relaxation dynamics of transient absorption spectra clearly indicates charge transfer state formation in the solid sample of 5-nitro substituted indolylcarbazole derivative.

KEYWORDS

Fischer indolization; density functional theory; ultrafast relaxation dynamics; charge transfer

Introduction

In recent years, electroluminescent [1, 2], photoluminescent [3] and nonlinear optical materials [4, 5] have attracted great attention due to their possible utilization in the different areas. There is an increasing demand for such type of high-performance materials particularly multi-functional opto-electronic materials. Most of such materials have fluorescent properties. In contrast to inorganic electro- and optically active materials their organic counterparts have advantages such as the relative ease of synthesis and processing, chemical and thermal robustness, possibility for further modification, and facile property tuning. Recently a great deal of attention is paid to bipolar organic materials consisting of electron donors (D), e.g. carbazole moiety, and electron acceptors (A), e.g. NO_2 or CN groups. The D-π-A arrangement assures efficient intramolecular charge transfer (ICT) between the donor and acceptor moieties.

The purpose of this work was synthesis and studies of the derivatives of indole and carbazole having vinylbenzyl groups and estimation of the influence of electron accepting nitro groups on the properties of the derivartives. The properties of the materials were investigated by means of thermal, electrochemical tools, steady-state and dynamic spectroscopy as well as by computational methods. It was presumed that the structural features may influence packing of the molecules and conseqyently charge transfer states formation. Furthermore, the position of nitro groups was found to have the most significant effect on the intramolecular charge transfer.

CONTACT J. V. Grazulevicius juozas.grazulevicius@ktu.lt
Color versions of one or more of the figures in the article can be found online at www.tandfonline.com/gmcl.

1. Experimental

1.1. Materials

Carbazole, acethyl chloride, aluminum chloride, benzyltrimethylamonnium hydrogensuphate, 2-ethylhexylbromide, iron (III) chloride, *m*-nitroaniline, phenylhydrazine, *p*-nitrophenylhydrazine, potassium *tert*-butoxide, 4-vinylbenzyl chloride (all from Aldrich), hydrogen chloride 37%, potassium hydroxide, (from Chempur), were used as received.

9-(2-Ethylhexyl)carbazole (**2**) was synthesized according to the known procedure [6].

3,6-Diacetyl-9-(2-ethylhexyl)carbazole (**3**) was synthesized according to the known procedure [7].

3-Acetyl-6-(1H-4-nitroindol-2-yl)-9-(2-ethylhexyl)carbazole (**4**). To a mechanically stirred solution of *m*-nitroaniline (1.16 g, 8.4 mmol) and 3,6- diacethyl-9-(2-ethylhexyl)carbazole **3** (0.5 g, 1.4 mmol) in dimethyl sulfoxide (DMSO) (10 ml), which was cooled down to 0-5°C degrees, potassium *tert*-butoxide (0.673 g,7 mmol) was added slowly. The reaction mixture was stirred at room temperature for 4 h. The reaction was stopped by pouring the reaction mixture into saturated NH_4Cl solution. The precipitate was filtrated and washed with water. The product was purified by silica gel column chromatography using dichloromethane as an eluent and isolated by precipitation in petroleum ether. Yield of dark red powder was 0.114 g (17%). M = 481g/mol.$C_{30}H_{31}N_3O_3$. MS (ESI) m/z:482 $[M+H]^+$.^{1}H NMR (300 MHz, $CDCl_3$) δ 11.87 (s, NH, 1H), 8.85 (d, J = 1.5 Hz, Ar., 2H), 8.76 (dd, J = 5.2, 3.8 Hz, Ar., 3H), 8.11 (ddd, J = 11.1, 7.8, 2.4 Hz, Ar., 1H), 7.82 – 7.75 (m, Ar., 1H), 7.58 (s, Ar., 3H), 7.51 – 7.41 (m, Ar., 1H), 7.20 (t, J = 8.0 Hz, Ar., 1H), 4.23 (d, J = 7.5 Hz, C$\underline{H}_2$, 2H), 2.75 (s, C$\underline{H}_3$, 3H), 2.04 (m, C$\underline{H}$, 1H), 1.35 (m, C$\underline{H}_2$, 8H), 0.88 (m, C$\underline{H}_3$, 6H).

3-Acetyl-6-(1H-5-nitroindol-2-yl)-9-(2-ethylhexyl)carbazole (**5**). Compound **3** (0.5 g,1.4 mmol) and *p*-nitrophenylhydrazine (0.858 g, 5.6 mmol) were mixed together and stirred at 100°C. Hot methane esulphonic acid (3.18 ml, 49 mmol) was added dropwise and stirred for additional 40 min. The reaction was stopped by pouring the reaction mixture into ice water; precipitate was then filtrated, washed with water. The product was purified by silica gel column chromatography using dichloromethane as an eluent and precipitated in methanol. Yield of red powder was 0.306 g (45%). M = 481g/mol. $C_{30}H_{31}N_3O_3$. MS (ESI) m/z:1025 $[2*M+OAc^-]^+$. ^{1}H NMR (300 MHz, DMSO) δ 10.25 (s, NH, 1H), 9.01 (d, J = 1.5 Hz, Ar., 1H), 8.73 (dd, J = 15.7, 1.6 Hz, Ar., 2H), 8.32 – 8.00 (m, Ar., 5H), 7.79 – 7.52 (m, Ar., 2H), 7.42 (d, J = 9.1 Hz, Ar., 2H), 4.35 (d, J = 7.4 Hz, C$\underline{H}_2$, 2H), 2.75 (s, C$\underline{H}_3$, 3H), 2.01 (m, C$\underline{H}$, 1H), 1.51 – 1.04 (m, C$\underline{H}_2$, 8H), 0.92 – 0.67 (m, C$\underline{H}_3$, 6H).

3-Acetyl-6-(1H-indol-2-yl)-9-(2-ethylhexyl)carbazole (**6**). Compound **3** (0.5 g, 1.4 mmol) and phenylhydrazine (0.55 ml, 5.6 mmol) were mixed together and stirred at 100°C for 1 h. Then hot methanesulfonic acid (2.73 ml, 42 mmol) was added dropwise and stirred for additional 10 min. The reaction was stopped by pouring the reaction mixture into ice water, precipitate was then filtrated, washed with water. The product was purified by silica gel column chromatography using dichloromethane as an eluent and precipitated in methanol. Yield of red powder was 0.165 g (27%). M = 436 g/mol. $C_{30}H_{32}N_2O$. MS (ESI) m/z: 873 $[2^*M+H]^+$. ^{1}H NMR (300 MHz, DMSO) δ 11.58 (s, NH,1H), 8.67 (t, J = 17.0 Hz, Ar.,1H), 8.16 – 7.89 (m, Ar., 2H), 7.60 (ddd, J = 43.0, 24.0, 5.2 Hz, Ar., 7H), 7.17 – 6.83 (m, Ar.,4H), 4.34 (d, J = 7.2 Hz, C$\underline{H}_2$,1H), 2.75 (s, C$\underline{H}_3$, 3H), 2.16 – 1.80 (m, C$\underline{H}$, 1H), 1.42 – 1.00 (m, C$\underline{H}_2$, 8H), 0.84 (ddd, J = 19.7, 14.3, 7.0 Hz, C$\underline{H}_3$, 6H).

3-Acetyl-6-(1-(4-vinylbenzyl)-4-nitroindol-2-yl)-9-(2-ethylhexyl)carbazole (**7**) was prepared by the procedure similar to that described elsewhere [8]. To a mechanically stirred solution of

compound **4** (0.05 g, 0.1 mmol), DMSO (10 ml), potassium *tert*-butoxide (0.056 g, 0.5 mmol), tetrabuthylammonium hydrogen sulphate (0.004 g, 0.01 mmol) and 4-vinylbenzylchloride (0.032 ml, 0.2 mmol) were added. The resulting mixture was stirred at room temperature for 2 h. The reaction was stopped by adding water and neutralized with 10% HCl (8 ml) to pH 6–7. The crude product was extracted with dichloromethane several times (50 ml×3). The dichloromethane solution was washed with water, dried with anhydrous sodium sulphate, filtered and the solvent was evaporated. The product was purified by silica gel column chromatography using hexane as an eluent. Yield of red powder was 0.047 g, (78%). M = 597 g/mol. $C_{39}H_{39}N_3O_3$. MS: *m/z* 598 [$(M+H)^+$].^{1}H NMR (400 MHz, $CDCl_3$) δ 8.08 (s, Ar., 1H), 7.56 (s, Ar., 3H), 7.47 – 7.40 (m, Ar., 4H), 7.36 (t, J = 7.5 Hz, 5H), 7.20 (t, J = 8.0 Hz, Ar., 1H), 6.74(d, 2H, J = 1.68 Hz, –CH=$\underline{CH_2}$), 5.90 – 5.62 (m, –$\underline{CH}$=CH_2, 1H), 4.23 (d, J = 7.5 Hz, C$\underline{H_2}$, 2H),.75 (s, C$\underline{H_3}$, 3H), 2.20 – 1.67 (m, C$\underline{H}$, 1H), 1.45 – 0.98 (m, C$\underline{H_2}$, 8H), 0.93 m, C$\underline{H_3}$, 6H). ^{13}C NMR (101 MHz, $CDCl_3$) δ 181.05, 171.49, 166.44, 165.46, 153.87, 150.55, 144.53, 143.93, 141.59,139.56, 130.30, 127.66, 118.33, 100.10, 35.35, 30.68, 27.37, 25.71, 13.74, 9.44, 4.48, 2.74. FT-IR cm^{-1}: 3052 (ν C–H Ar), 2982 (ν C–H aliph.), 1705 (ν C=O aliph.), 1500 (ν nitro), 1497 (ν C=C Ar), 1351 (ν C–N Ar), 960, 902 (γ C–H aliph.).

3-Acetyl-6-(1-(4-vinylbenzyl)-5-nitroindol-2-yl)-9-(2-ethylhexyl)carbazole **8**. To a mechanically stirred mixture of compund **5** (0.05 g, 0.1 mmol), DMSO (15 ml), potassium *tert*-butoxide (0.056 g, 0.5 mmol), tetrabuthylammonium hydrogen sulphate (0.004 g, 0.01 mmol) and 4-vinylbenzylchloride (0.032 ml, 0.2 mmol) were added. The resulting mixture was stirred at room temperature for 24 h. The reaction was stopped by adding water and neutralized with 10% HCl (8 ml) to pH 6–7. The crude product was extracted with dichloromethane several times (50 ml×3). The dichloromethane solution was washed with water, dried with anhydrous sodium sulphate, filtered and the solvent was evaporated. The product was purified by silica gel column chromatography using hexane as an eluent. Yield of dark red powder was 0.044 g, (74%). M = 597 g/mol. $C_{39}H_{39}N_3O_3$. MS: m/z 599 [$(M+2H)^+$]. ^{1}H NMR (400 MHz, $CDCl_3$) δ 8.33 – 7.97 (m, Ar., 3H,), 7.94 – 7.79 (m, Ar., 2H), 7.67 – 7.48 (m, Ar., 5H), 7.07 – 6.76 (m, Ar., 4H), 6.67 (d, 2H, J = 1.68 Hz, -CH=$\underline{CH_2}$), 5.76 (m, –$\underline{CH}$=CH2, 1H,), 4.35 (d, J = 7.4 Hz, C$\underline{H_2}$, 2H), 2.75 (s, C$\underline{H_3}$, 3H), 2.05 (s, C$\underline{H}$, 1H), 1.27 (d, J = 7.3 Hz, C$\underline{H_2}$, 8H), 0.89 (ddd, J = 17.3, 12.7, 6.5 Hz, C$\underline{H_3}$, 6H).

^{13}C NMR (101 MHz, $CDCl_3$) δ 191.74, 189.03, 165.84, 157.86, 154.17, 149.88, 146.19, 137.23, 134.59, 128.27, 126.98, 32.03, 27.37, 24.35, 23.68,14.04, 11.10, 10.05. FT-IR cm^{-1}: 3012 (ν C–H Ar), 2995, 2982 (ν C–H aliph.), 1705 (ν C=O aliph.), 1502, 1499 (ν nitro), 1410 (ν C=C Ar), 1345, 1320 (ν C–N Ar), 955, 910 (γ C-H aliph.).

3-Acetyl-6-(1-(4-vinylbenzyl)indol-2-yl)-9-(2-ethylhexyl)carbazole **9**. To a mechanically stirred mixture of compound **6** (0.05 g, 0.1 mmol), DMSO (10 ml), potassium *tert*-butoxide (0.056 g, 0.5 mmol), tetrabuthylammonium hydrogen sulphate (0.004 g, 0.01 mmol) and 4-vinylbenzylchloride (0.032 ml, 0.2 mmol) were added. The resulting mixture was stirred at room temperature for 24 h. The reaction was stopped by adding water and neutralized with 10% HCl (8 ml) to pH 6–7. The crude product was extracted with dichloromethane several times (50 ml×3). The dichloromethane solution was washed with water, dried with anhydrous sodium sulphate, filtered and the solvent was evaporated. The product was purified by silica gel column chromatography using hexane as an eluent. Yield of dark red powder was 0.035g, (65%). M = 552 g/mol. $C_{39}H_{40}N_2O$. MS: m/z 551 [M^+].^{1}H NMR (400 MHz, $CDCl_3$) δ 7.46 d (J = 8.1 Hz, 2H), 7.41 – 7.33 (m, Ar., 8H), 7.17 – 6.71 (m, Ar., 4H), 6.60 (d, 2H, J = 1.68 Hz, –CH=$\underline{CH_2}$), 5.75 (m, –$\underline{CH}$=CH_2, 1H), 4.34 (d, J = 7.2 Hz, C$\underline{H_2}$,1H), 2.75 (s, C$\underline{H_3}$, 3H), 2.16 – 1.80 (m, C$\underline{H}$, 1H), 1.51 – 0.95 (m, C$\underline{H_2}$, 8H), 0.98 – 0.65 (m, C$\underline{H_3}$, 6H). ^{13}C NMR (101 MHz, $CDCl_3$) δ 180.45, 177.13, 137.60, 135.57, 129.32, 128.94, 124.95, 114.33, 111.70,

66.22, 63.89, 33.99, 30.30, 29.72, 24.35, 20.74, 14.04, 13.06, 12.08. FT-IR cm^{-1}: 3002 (ν C–H Ar), 2995, 2911 (ν C–H aliph.), 1708 (ν C=O aliph.), 1499, 1482 (ν C=C Ar), 1351, 1298 (ν C–N Ar), 990, 960, 902 (γ C-H aliph.).

1.2. Instrumentation

^{1}H and ^{13}C NMR spectra were obtained using a Bruker Avance III (400 MHz). The data are given as chemical shifts (δ) in ppm against trimethylsilane (in parenthesis: multiplicity, integration, coupling constant). IR spectra were recorded using a Vertex 70 Bruker spectrometer. Mass spectra were obtained on a Waters ZQ 2000 mass spectrometer (electron spray ionization). Elemental analysis was performed with an Exeter Analytical CE-440 Elemental Analyzer. UV spectra of the dilute tetrahydrofuran, toluene and acetonitrile solutions (10^{-4} M) and of thin films on quartz plates of the synthesized compounds were recorded with Avantes Avaspec 2048XL spectrophotometer. Fluorescence spectra of the dilute tetrahydrofuran, toluene and acetonitrile solutions (10^{-4} M) and of thin films on quartz plates, fluorescence decays of the dilute tetrahydrofuran (10^{-4} M) solutions of the synthesized materials were recorded with Edinburgh Instruments FLS980 spectrometer at room temperature (excitation wavelengths $\lambda_{ex} = 290$ nm and 400 nm). For fluorescence decay measurements Xenon flashlamp μF920H with time resolution of 200 ps (excitation wavelength $\lambda_{ex} = 420$ nm) was used. Ultrafast excited-state relaxation processes of the dilute tetrahydrofuran and toluene solutions (10^{-4} M) and of thin films on quartz plates of the synthesized compounds were tested using ultrafast Yb:KGW laser Pharos (Light Conversion) with a regenerative amplifier generating 200 kHz repetition rate 290 fs duration pulses at 1030 nm wavelength. The proper excitation wavelength chosen from the highest absorption amplitude in the steady state absorption spectra in most cases was tuned at 415 or 430 nm with a collinear optical parametric generator Orpheus and harmonic generator Lyra (Light Conversion). The samples were probed with a white light supercontinuum generated using 2 mm thick sapphire plate excited with the fundamental laser wavelength at 1030 nm. The spectral range of supercontinuum as well as the detection range of the transient absorption spectra dynamics was from 480 nm to 800 nm. The excitation beam was focused to a spot of about 700 μm in diameter, while the probe white light supercontinuum beam diameter was of about 500 μm. Differential scanning calorimetry (DSC) measurements were carried out using a DSC Q 100 TA Instrument thermosystem. The samples were examined at a heating/cooling rate of 10 °C/min under nitrogen atmosphere. Thermogravimetric analysis (TGA) was performed on a Metter TGA/SDTA851e/LF/1100 apparatus. The heating rate was 20 °C/min. The measurements were done under nitrogen atmosphere. The melting points of the compounds were determined using an Electrothermal MEL-TEMP. Cyclic voltammetry (CV) measurements were performed using a glassy carbon working electrode (disk with the diameter of 2 mm) in a three-electrode cell using an Autolab Type potentiostat-galvanostat. The measurements were carried out for the solutions in dry dichloromethane containing 0.1 M tetrabutylammonium hexafluorophosphate at 25 °C (scan rate 50 mV/s, sample concentration 10^{-3} M). The potentials were measured against Ag wire as reference electrode. Platinum wire was used as a counter electrode. The potentials were calibrated with the standard ferrocene/ferrocenium (Fc/Fc^{+}) redox system [9]. The density functional theory (DFT) calculations were carried out with the Spartan'14 program [10] while the time-dependent DFT (TD-DFT) calculations were carried out with Gaussian 09 software package [11]. The calculations were optimized by means of the B3LYP (Becke three parameters hybrid functional with Lee-Yang-Perdew correlation functionals) [12] with the 6/31G (d, p) atomic basis set.

2. Results and discussion

The synthetic routes to indolyl-substitutes carbazole derivatives are shown Scheme 1. Two types of reactions i.e. Makoszha reaction [13] and Fischer indolization [14] were employed. These methods were found to be the most efficient because of the inexpensive reagents and simple reaction conditions. The acetylated carbazole derivative was treated with *m*-nitroaniline to form a 4-nitro substituted indole ring. The reaction was carried out in DMSO with potassium *tert*-butoxide at room temperature. To obtain 5-nitro substituted derivative (**5**) and compound **6**, the acetylated carbazole was treated with *p*-nitrophenylhydrazine or phenylhydrazine respectively. The reactions were catalyzed by methanesulphonic acid. The target products **7**-**9** were obtained by the treatment of compound **5**-**6** in the presence of potassium tert-butoxide and tetrabuthylammonium hydrogen sulphate.

All the target products were purified by adsorption chromatography and fully characterized by IR, ^{1}H NMR, ^{13}C NMR and mass spectroscopies, which confirmed their expected molecular structures. The compounds were soluble in common organic solvents.

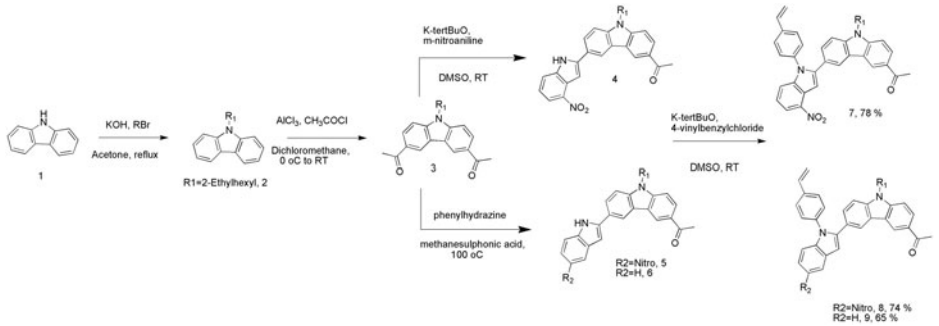

Scheme 1. Synthesis indolyl-substituted carbazole derivatives.

Thermal properties of the derivatives were investigated by thermogravimetric (TG) analysis and differential scanning calorimetry (DSC). The thermal characteristics of compounds **7**–**9** are collected in Table 1. The thermal stability the indolyl-substituted carbazole compounds was found to be rather moderate. Their 5% weight loss temperatures were found to be in the range from 290°C to 350°C. Derivatives containing nitro group attached to the indole moiety (**8** and **9**) showed higher 5% weight-loss temperatures as compared to the derivative **9** having no nitro group. The final compounds **7**–**9** were isolated as amorphous materials. There were no signals of melting or crystallization observed during the DSC measurements. Compounds **7**–**9** were found to be capable of the formation of molecular glasses. Their glass transition temperatures were found to be around 60°C.

Electrochemical properties of the compounds were investigated by cyclic voltammetry (CV). The resulting data are summarized in Table 1. As an example, cyclic voltammogram of compound **8** is shown in Fig. 1.

All the studied compounds showed irreversible oxidation. Irreversible oxidation was followed by coupling of indole radical cations apparently because of high reactivity of indole moiety at C-3 position. The solid-state ionization potential (IP_{CV}) and electron affinity (EA_{CV}) values were estimated from the oxidation onset potentials ($E_{ox\ onset\ vs.Fc}$) and optical band gaps (E_g^{opt}). The ionization potential values of compounds **7**–**9** established by CV were found to be in the short range of 5.51–5.61 eV. The electron affinity values ranged from 2.90 to 3.14 eV. The theorical energies of HOMO and LUMO of **7**–**9** were calculated using DFT/B3LYP/6/31

Table 1. Thermal, photophysical and electrochemical properties of nitro substituted indolylcarbazole derivatives 7–9.

Compound	**7**	**8**	**9**
T_G [a], °C	62	— [b]	59
$T_{D\text{-}5\%}$ [c], °C	350	340	290
Solution			
λ_{Abs} [d], nm	412	416	410
λ_{PL} [e], nm	525	537	530
Stokes shift[f], nm	113	121	120
E_G^{opt} [g], eV	2.54	2.47	2.61
$E_{oxonsetvsFc}$ [h], V	0.49	0.51	0.41
IP_{cv} [i], eV	5.59	5.61	5.51
EA_{cv} [j], eV	3.05	3.14	2.90
E_{HOMOT} [k], eV	−5.63	−5.61	−5.08
E_{LUMOT} [l], eV	−2.10	−1.83	−1.19
$T_{D\text{-}5\%}$ [a], °C	350	340	290
λ_{Abs} [b], nm	412	416	410
λ_{PL} [c], nm	525	537	530
Stokes shift[d], nm	113	121	120
E_G^{opt} [e], eV	2.54	2.47	2.61
$E_{oxonsetvsFc}$ [f], V	0.49	0.51	0.41
IP_{cv} [g], eV	5.59	5.61	5.51
EA_{cv} [h], eV	3.05	3.14	2.90
E_{HOMOT} [i], eV	−5.63	−5.61	−5.08
E_{LUMOT} [j], eV	−2.10	−1.83	−1.19

[a] – glass transition from DSC curves;
[b] – not detected;
[c] – 5% weight loss temperature obtained from TG curves;
[d] – absorption maxima;
[e] – emission maxima;
[f] – λ_{Fl}-λ_{Abs};
[g] – optical band gap calculated from 1240/$\lambda_{Absonset}$ (onset absorption);
[h] –onset oxidation potential of the sample vs. onset oxidation potential of ferrocene;
[i] – ionization potencial, $IP_{CV} = E_{onset\ ox\ vs.Fc} + 5.1$ eV [i, ii];
[j] – electron affinity, $EA_{CV} = IP_{CV} - E_g^{opt}$;
[k] – theoretically calculated HOMO level energy;
[j] – theoretically calculated LUMO level energy.

(d, p) method. The energies of HOMO and LUMO for **7** were found to be −5.63 eV and −2.10 eV, respectively, those observed for **8** were −5.61 eV and - 1.83 eV, respectively, and those for **9** were -5.08 eV and −1.19 eV, respectively. The comparable values of IP as well as HOMO energies proves that the addition of nitro group to the molecule hightens its polarity. Furthermore, a slight difference between the values of the electrochemical characteristics of both compounds containing nitro groups (**7** and **8**) shows the influence of the conjugation arrangement of the nitro group.

The steady-state absorption and fluorescence spectra of the solutions in THF of **7**/**9** are shown in Figure 2a. The maxima of absorption spectra of the films and solutions were observed at the similar wavelengths (Fig. 2b).

We also have measured absorption spectra of the solutions of **7**-**9** in the solvents of the different polarity. Toluene, tetrahydrofuran and acetonitrile were used as the solvents. In general, absorption spectra were quite similar.

The fluorescence spectra were found to be much more sensitive to the environment than absorption spectra (Fig. 2a). The fluorescence spectra of the solutions of **7**-**9** in THF have one

[i] Cardona, C. M., Li, W., Kaifer, A. E., Stockdale, D., Bazan, G. C. (2011). *Adv. Mater., 23*, 2367.
[ii] Rybakiewicz, R., Gawrys, P., Tsikritzis, D., Emmanouil, K., Kennou, S., Zagorska, M., Pron, A. (2013). *Electrochim. Acta, 96*, 13.

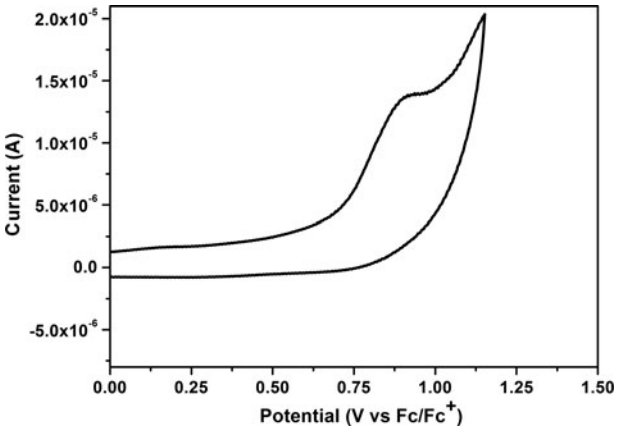

Figure 1. Cyclic voltammogram of compound 8.

clear fluorescence band only at 550 nm. The fluorescence spectrum of the solution of compound **8** in THF shows some differences from the spectra of the THF solutions of the other samples (Fig. 2a). The fluorescence spectrum of the solution of **8** is red shifted in comparison to the spectra of the solutions of compounds **7** and **9** and it does not have shoulder below 450 nm. This may show some structural differences in these samples.

The complex structures of fluorescence spectra indicate multiple structure of energy levels in molecules of compounds **7**-**9** (Figure 2). In order to investigate this more deeply, transient absorption spectra were recorded for the films and solutions in THF (Figure 3, 5). The transient absorption spectra dynamics of **8** showed most interesting results both for films and solutions.

Transient absorption spectra of **8** in THF solution show four peaks: two peaks of positive and negative signal. The stimulated emission signal decreases at 550 nm and evidently that also causes the increase of another signal at 620 nm. During the excited state relaxation dynamics the energy is transferred from energy level attributable to wavelength of 550 nm to 620 nm. The peak at 550 nm is similar to steady-state fluorescence showing that 550 nm can be attributed to fluorescence from lowest excited state level S_1. 620 nm can be attributed to another lower energy level like dimmers of J-aggregates type.

After deeper analysis of sample **9** we can say that **9** solution in THF has some similarities to **8**. In its transient absorption spectra only positive signal can be seen at first (delay time

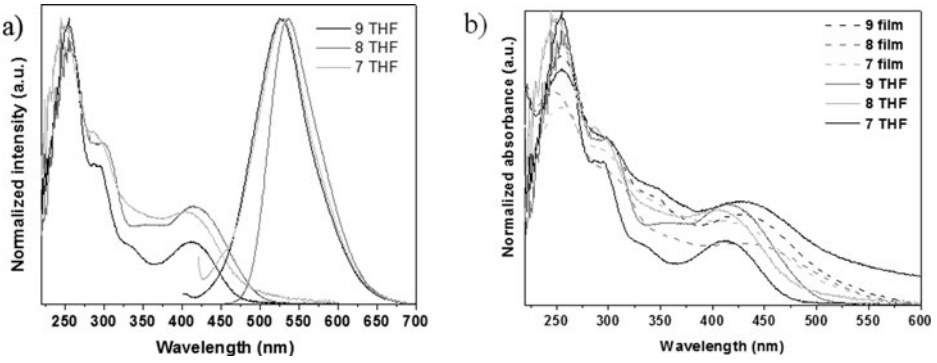

Figure 2. Steady-state absorption and fluorescence spectra measured of (7/9) samples solution in THF (a) and absorbtion spectra of the solutions and thin films of compounds 7/9 (b). Excitation wavelength 400 nm.

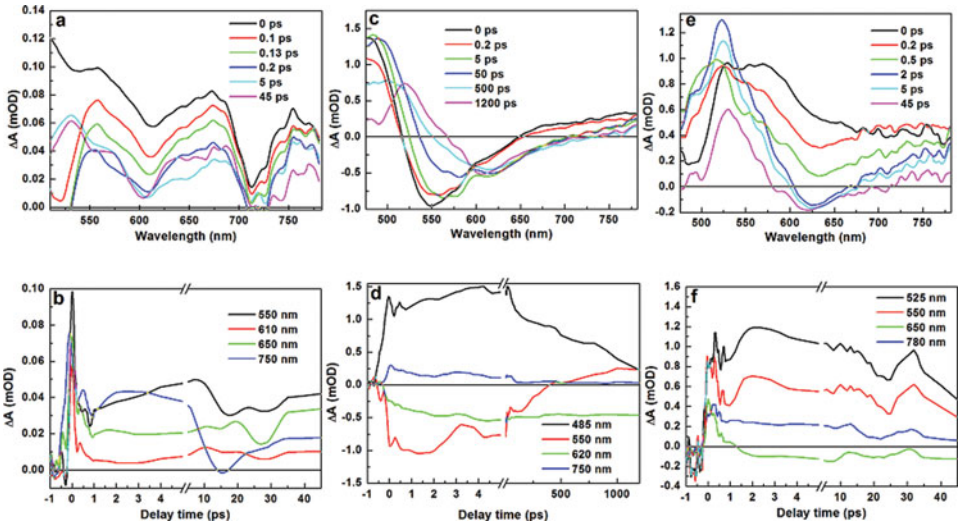

Figure 3. Transient absorption spectra and kinetics of 7 (a, b), 8 (c, d), 9 (e, f) in solution of THF. Wavelength of excitation 415 nm, intensity 3.9 mW.

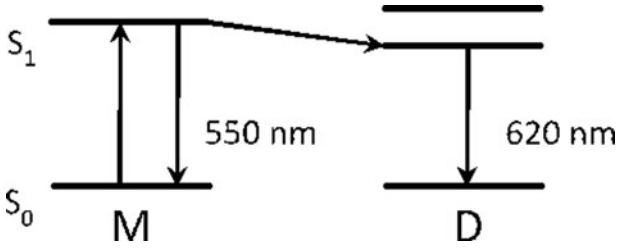

Figure 4. Energy level diagram that describes energy relaxation in THF and Toluene solutions of compound 8. Simplified energy levels of (8, 9): M-shows energy levels of monomer and D-shows energy levels of J-type aggregated dimer. Arrows down indicates stimulated emission at 550 and 620 nm; arrow up indicates absorption. Stokes shift is not included in this scheme.

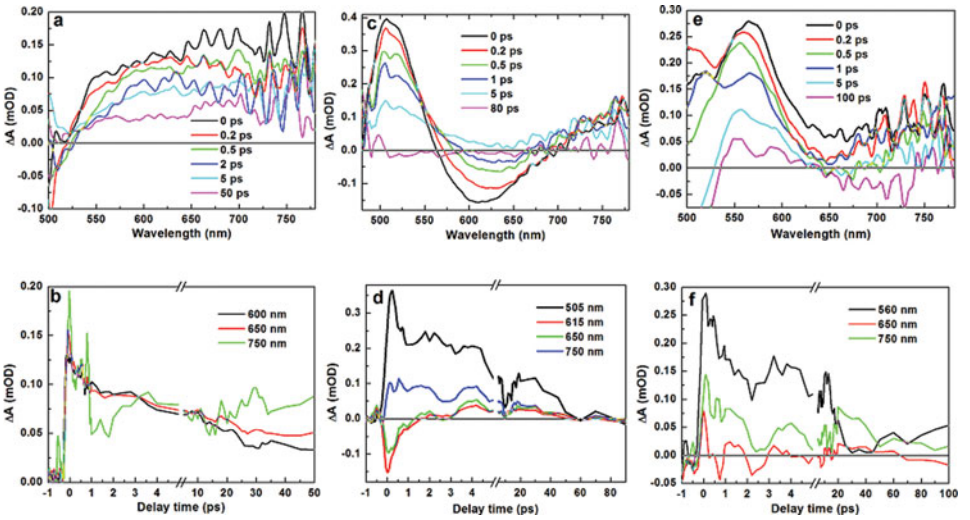

Figure 5. Transient absorption and absorption kinetics spectra of thin films of 7 (a, b), 8 (c, d), 9 (e, f). Wavelength of excitation 430 nm, intensity 4.4 mW.

Table 2. Properties of the selected transitions and their contribution to the UV-vis spectra of the derivatives 7–9 calculated at the B3LYP/6-31G(d,p)/PCM(THF) level.

Compound	Calculated wavelengths of UV absorption bands, nm	Oscillator strength, a.u.	Major contribution
7	328	0.2741	H→L+1 (92%)
	286	0.3826	H-1→L+1 (42%)
8	443	0.3740	H→L (98%)
	347	0.4207	H→L+1 (91%)
	265	0.4976	H-2→L+2 (65%)
9	350	0.6880	H→L+1 (91%)
	309	0.1759	H-1→L+1 (44%)
	248	0.4408	H-1→L+3 (42%)

0 ps). After more than 1 ps, negative signal appears at 625 nm. It has analogy to the same signal at 620 nm in **8** sample and perhaps can be attributed to the same kind of lower energy level because of dimmers of J-aggregates type. The stimulated emission cannot be seen for monomers perhaps because this signal is overrun by induced absorption, but one can clearly see the rise of new negative signal that can be attributed to the energy transfer to new molecular species. That shows that **8**-**9** molecules are prone to form J-aggregates [15]. Sample **7** in THF solution does not show any complex relaxation dynamics. Transient absorption spectra of **7** in both cases: in solutions of THF and films have low transient absorption signal (Figure 3).

Dynamic fluorescence measurements were also done for **7**-**9** samples in THF solution. The calculated lifetimes are summarized in Table 2.

In all three samples we can see a similar tendency of fluorescence relaxation that at shorter wavelengths it is a bit faster than at longer. This may correspond to energy transfer form monomers to dimers. The difference is small but clear.

The energy transfer process is much more clearly observed in pump-probe measurements, probably because of much higher pump-probe temporal resolution. It is 0.3 ps for pump-probe and 200 ps for our fluorescence decay measurements. That is why we prefer pump-probe measurements data in our research data analysis. The energy transfer process is shown in Figure 4.

There are three transient absorption peaks in transient absorption spectrum of **8** film, two positive and one negative peaks (Figure 5c). The negative peak, according to steady-state fluorescence spectra, can be attributed to stimulated emission while the other two can be ascribed to the induced absorption. The origin of negative signal is quite clear but the explanation of positive signal is much more complicated and will not be discussed more deeply in this article.

In order to describe the relaxation dynamics we have analyzed relaxation kinetics of the absorbtion of the compounds **7**-**9** (Fig. 5d) in more detail. The kinetics at the most characteristic points of transient absorption were analyzed (505, 615 and 750 nm). A fast relaxation

Table 3. Fluorescence relaxation lifetimes and amplitudes of 7-9 samples in solutions. Samples were excited at 420 nm wavelength.

Sample	Wavelength of decay analysis, nm	τ_1	A_1	τ_2	A_2
7	550	0.52	52.98	2.95	47.02
	620	0.63	52.01	3.32	47.99
8	545	0.87	18.70	2.80	81.30
	620	1.07	20.73	2.65	79.27
9	540	0.35	57.28	2.95	42.72
	600	0.41	56.88	3.24	43.12

τ_1 and τ_2 - decay times of relatively fast and slow components; A_1 and A_2 - amplitudes of decay components.

component can be seen in both positive and negative signals while positive signal also has a slower relaxation component. This signal of stimulated emission spectra can be attributed to fluorescence from energy level S_1. The disappearance of this signal means that there are no molecules excited to S_1 energy level, while remains of the positive signal suggest that molecules did not relax to the ground state level. Evidently, that means that the relaxation take place to new energy level that is below S_1. No negative signal can be seen after 1 ps. This observation indicates that molecules have relaxed to a state of low transition dipole moment from which fluorescence is very inefficient. It is worth to mention that charge transfer states have low transition dipole moment, therefore we may suggest that molecules have formed charge transfer states. Despite quite similar structure, the samples **7** and **9** show more simple relaxation dynamics without stimulated emission signal.

For the comparison, transient absorption spectra of the solutions of **7**-**9** in THF and toluene were recorded. In the case of **8**, transient absorption spectra relaxation dynamics was found to be the most complex. Despite usual excited state relaxation dynamics, another processes like charge transfer state formation were observed.

Ultrafast relaxation dynamics of **8** in the form of films may show formation of charge transfer states, while in the solutions energy transfer from molecules to dimmers may take place. This observation indicates that charge transfer states are formed only in the films when molecules are packed quite close, suggesting that dense packing is essential for the formation of charge transfer states. This means that the observed charge transfer is an intermolecular process. It is obvious from the data given in Figure 5 that the relaxation time of excited states is less than 100 ps. These results suggest fast quenching of the excited state. The level diagram shown in Figure 4 cannot be applied to the films. More complex energy level structure in the films is expected.

In order to get more insight into the nature of the absorption bands of **7**–**9**, TD-DFT calculations were performed. The excitation energies and oscillator strengths of the optimized structures of the molecules **7**–**9** are presented in Table 2. Theoretical UV-vis spectra are shown in Figure 6.

Compound **7** has two significant energy bands in the UV-vis spectrum. The first excitation with the oscillator strength of 0.2741 corresponds to the HOMO→LUMO + 1 transition. This transition is from the whole molecule to 3-acetylcarbazole unit excluding nitro group at C-4 position of the indole moiety. Therefore, this excitation corresponds to π-π^* transition for both conjugated chromophores. Compound **8** has three absorption bands in its UV-vis spectrum. The first excitation with the oscillator strength of 0.3740 corresponds to the HOMO→LUMO transition. This transition is towards nitro group at C-5 position of indole moiety. This transition can be ascribed to the intramolecular charge transfer. The excitation with the oscillator strength of 0.4207 corresponds to the HOMO→LUMO + 1 transition. This transition is localized on carbazole unit and its C-3 position substituent i.e. acetyl group.

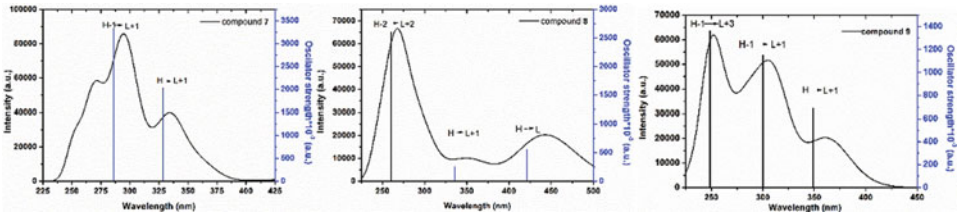

Figure 6. Calculated UV-vis spectra of compounds 7-9 at the B3LYP/6-31G(d,p)/PCM(THF) level; bars represent oscillator strength.

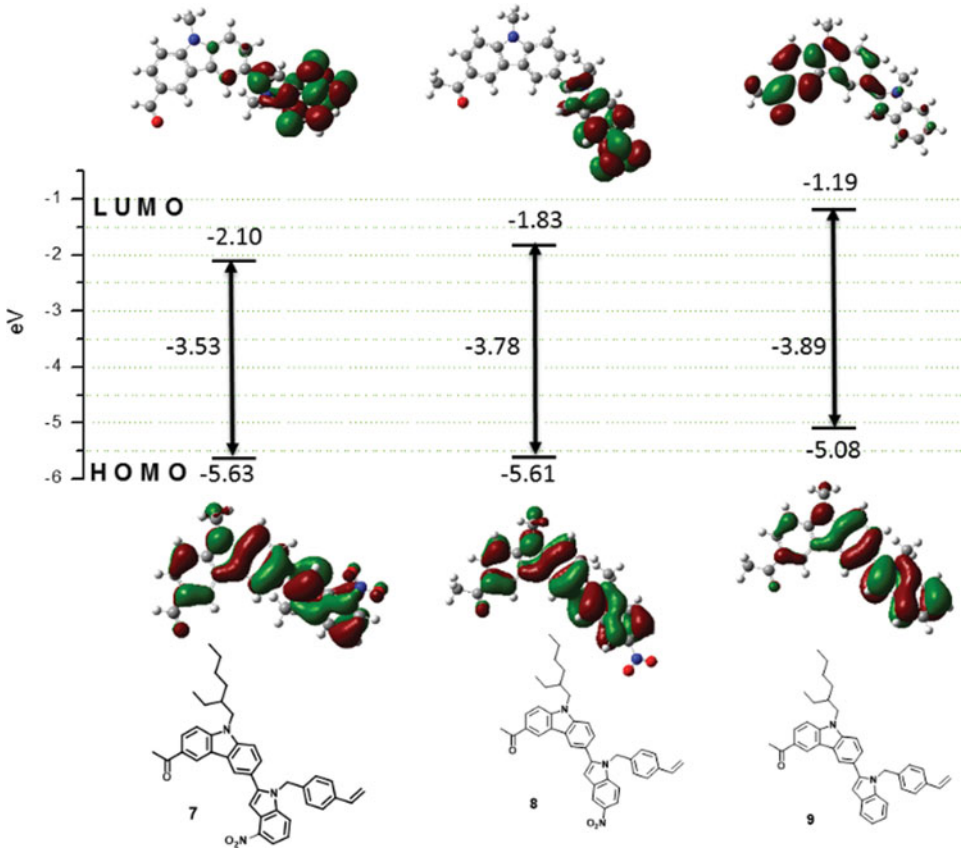

Figure 7. The computed spatial distributions of HOMO and LUMO orbitals for derivatives 7–9.

Compound **9** also has three absorption bands. The first excitation with the oscillator strength of 0.6880 corresponds to the HOMO→LUMO + 1 transition. This transition is localized on carbazole unit.

Different molecular behavior of compounds **7** and **8** upon excitation is determined by their structures. Nitro group is in the main conjugation system of compound **8**. This makes intramolecular charge transfer possible and dependant on the linking topology of the nitro group. Whereas, nitro group at C-4 position of indole moiety is excluded from the main conjugation system of the molecule **7** which leads to the charge transfer towards carbazole moiety (Figure 7). The molecule orbital transition behavior of compound **9** is rather similar to that of compound **7**.

Conclusions

A series of new indolyl-substituted carbazole derivatives were synthesized and their properties were studied. All the final compounds form molecular glasses. They absorb electromagnetic radiation in the range of 200–400 nm and emit in the range of 420–600 nm. Dynamics of transient absorption relaxation spectra clearly indicates charge transfer state formation in solid state sample of 5-nitro substituted indolylcarbazole derivative. The structural features may influence packing of the molecules and therefore charge transfer states formation. The

linking topology of nitro groups was found to be the most significant on intramolecular charge transfer.

Acknowledgment

This research was funded by a grant (No. MTEPI-P-16025) from the R&D and Innovation Fund of Kaunas University of Technology.

References

[1] Zhang, W., He, Z., Mu, L., Zou, Y., Wang, Y., & Zhao, S. (2010). *Dyes Pigm.*, *85*, 86.
[2] Giovanella, U., Botta, C., Bossi, A., Licandro, E., & Maiorana, S. (2006). *J. Appl. Phys.*, *100*, 83107.
[3] Hoshimoto, M., Igawa, S., Yashima, M., Kawata, I., Hoshino, M., & Osawa, M. (2011). *J Am Chem Soc.*, *133*, 10348.
[4] Belfield, K. D., Hagan, D. J., Stryland, E. W. V., Schafer, K. J. C., & Negres, R. (1999). *Org Lett.*, *1*, 1575.
[5] Verma, R., Dhar, R., Rath, M. C., Sarkar, S. K., & Dabrowski, R. (2012). *J Phys Chem Solids*, *73*, 288.
[6] Brunner, K., Dijken, A., Börner, H., Bastiaansen, J., Kiggen, N., & Langeveld, B. (2004). *J Am Chem Soc.*, *19*, 6035.
[7] Hao, L. L., Li, J.F., Lin, P. H., Dong, R. F., Li, D. X., Shuang, S. M., & Dong, C. H. (2010). *Chin. Chem. Lett.*, *21*, 9.
[8] Kruzinauskiene, A., Matoliukstyte, A., Michaleviciute, A., Grazulevicius, J. V., Musnickas, J., Gaidelis, V., & Jankauskas, V. (2007). *Synth. Met.*, *157*, 401.
[9] Gritzner, G., & Kuta, J. (1984). *Pure Appl. Chem.*, *56*, 461.
[10] SPARTAN'14 for Windows Version 1.1.2. 1840 Von Karman Avenue, Suite 370, Irvine, CA 92612: Wavefunction, Inc.; 2013.
[11] Frisch, M. J., Trucks, G. W., Schlegel, H. B., Scuseria, G. E., Robb, M. A., Cheeseman, J. R., & Fox, D. J., et al. Wallingford CT: Gaussian, Inc; 2009.
[12] Becke, A. D. (1988). *Phys Rev A*, *38*, 3098.
[13] Moskalev, N., Barbasiewicz, M., & Mąkosza, M. (2004). *Tetrahedron*, *60*, 347.
[14] Sengul, I. F., Wood, K., Kumar, N., & Black, D. St. C. (2012). *Tetrahedron*, *68*, 9050.
[15] Kazakevičius, A., Peckus, D., Boiko, O., Valkunas, L., Leonenko, E., Telbiz, G., & Gulbinas, V. (2015). *J. Phys. Chem. C*, *119*, 19126.